JCTC Journal of Chemical Theory and Computation

# Simulating Membrane Dynamics in Nonhomogeneous Hydrodynamic Environments

Lawrence C.-L. Lin† and Frank L. H. Brown*,‡

*Department of Physics, University of California, Santa Barbara, California 93106-9530, and Department of Chemistry and Biochemistry, University of California, Santa Barbara, California 93106-9510*

Received November 28, 2005

**Abstract:** Two previously introduced simulation algorithms for the dynamics of elastic membrane sheets embedded in a fluid medium are extended to account for inhomogeneous hydrodynamic environments. We calculate the height autocorrelation function for a lipid bilayer randomly pinned to a flat substrate and the influence of fluid confinement by the spectrin cytoskeleton on short wavelength membrane undulations of the human red blood cell. Altering the hydrodynamic environment of the membrane leads to significant changes in dynamics, and we discuss these effects in the context of recent experiments.

## I. Introduction

Many interesting problems in membrane biophysics, cellular biology, and biochemistry involve length and time scales completely inaccessible to molecular dynamics simulation. Simple estimates[1] indicate that it will be several decades before fully atomic models will become viable tools for studying lipid bilayers over the micron and millisecond scales necessary to make connection with cellular scale behavior. Recent progress in developing coarse-grained lipid models[2−19] points to a more optimistic future for molecular simulation of biomembranes and related materials; however, these methods are still far too computationally intensive for practical use in studying length scales exceeding tens of nanometers and time scales exceeding hundreds of nanoseconds. Elastic models represent the only theoretical/computational means presently available for studying biomembranes and lipid bilayers over long length and time scales.

The traditional Canham-Helfrich elastic picture for membrane energetics[20−22] combined with overdamped dynamics in a hydrodynamic environment[23,24] has been successfully applied to numerous biophysical questions of interest. However such considerations are typically limited to problems simple enough to be treated analytically[23,25−27] or problems where dynamics are not explicitly considered.[28−31] Recently, we have proposed two simulation algorithms for studying the dynamics of membranes evolving under the influence of perturbations that do not allow for analytical treatment. The first of these methods is specific to harmonic potentials where it is possible to numerically (but impossible analytically) identify the normal modes of the system.[32] The second method is applicable to general anharmonic potentials.[33,34] We will refer to both of these methods as Fourier space Brownian dynamics (FSBD) in this work.

Both of the previously introduced FSBD algorithms have solved for the dynamics of elastic sheets residing in a fluid medium of infinite extent. More realistically, biological cells and the artificial systems developed to mimic biomembranes reside in finite environments, which can act to constrain the fluid flow proximal to the membrane surface. While this fact is appreciated in the theory literature,[23,35,36] we are unaware of prior simulations that have incorporated the effect of finite sized hydrodynamic environments. It turns out that our existing FSBD methodology may be extended to account for impermeable walls near a dynamically evolving membrane with little difficulty. The purpose of this article is to describe the necessary extensions to FSBD to model a dynamically fluctuating membrane near a wall impermeable to fluid flow. Similar considerations can be applied to semipermeable walls[38] as well.

The effect of altering the hydrodynamic environment around the membrane surface can be striking. Although the

* Corresponding author phone: (805)893-5494; fax: (805)893-4120; e-mail: flbrown@chem.ucsb.edu.
† Department of Physics.
‡ Department of Chemistry and Biochemistry.

10.1021/ct050293s CCC: $33.50 
Published on Web 03/08/2006

thermal statistics of the membrane are not altered (as the energetics of the system do not change), the dynamics involved in sampling configurations can be modified by orders of magnitude. Physically, this effect is due to the difficulty in moving an incompressible fluid around inside a small volume and could be anticipated; however, the effect is surprisingly large and demonstrates the importance of including hydrodynamic effects properly in any simulation. For the purposes of illustration, we model the height−height correlation function of a membrane pinned to a solid support as seen in recent experiments[37,38] and show that the inclusion of an impermeable wall in the treatment slows dynamics by several orders of magnitude relative to treatments that ignore the presence of the solid support. Our results are in general agreement with experiment. We also consider the effect of hydrodynamic effects on the fluctuation dynamics of the red blood cell and related consequences for membrane protein diffusion. These results are compared to prior studies where such effects were neglected and significant influence of hydrodynamics is noted.

## II. Background: Energetics and Dynamics of an Fluid Membrane Sheet

We begin by specifying the Hamiltonian for a thin membrane sheet. For the systems we study in this work, it is valid to assume that the bilayer is nearly flat and height fluctuations normal to the plane of the membrane are small. In this case, a convenient parametrization is the Monge gauge, which specifies the height of the membrane $h(\mathbf{r})$ in terms of the location $\mathbf{r} \equiv (x, y)$ in the $xy$ plane. The total energy is therefore written as (Canham-Helfrich energetics)[20−22]

$$H = \int_A d\mathbf{r} \left\{ \frac{\kappa}{2}[\nabla^2 h(\mathbf{r})]^2 + \frac{\sigma}{2}[\nabla h(\mathbf{r})]^2 + \mathscr{H}_{\text{int}}[h(\mathbf{r})] \right\} \quad (1)$$

where $\kappa$ is the bending modulus, $\sigma$ is the surface tension, and $A = L^2$ is the projected area of a square patch of membrane. The height $h(\mathbf{r})$ is taken to be periodic with period $L$ in both the $x$ and $y$ directions. The first two terms of $H$ reflect bending energetics and energetics due to surface tension. These terms will be present even for an isolated membrane sheet suspended in solution. The last term allows for arbitrary functional dependence of $H$ on $h(\mathbf{r})$ as dictated by any interactions between the membrane and its environment.

In the overdamped regime appropriate to cellular scale dynamics,[39] the velocity field of the membrane is expected to be linearly dependent upon the forces acting on the sheet.[40] The relationship is generally nonlocal in space due to hydrodynamic interactions between distant points on the membrane surface.[40] Assuming that height fluctuations away from $h(\mathbf{r}) = 0$ are small, the expression for membrane velocity is[24]

$$v_m(\mathbf{r}, t) = \frac{\partial h(\mathbf{r}, t)}{\partial t} \quad (2)$$

$$= \int_{-\infty}^{\infty} d\mathbf{r}' \, \Lambda(\mathbf{r} - \mathbf{r}')[F(\mathbf{r}', t) + \zeta(\mathbf{r}', t)]$$

where $F(\mathbf{r}, t) = -\delta H/\delta h(\mathbf{r}, t)$ is the force per area on the membrane resulting from the Hamiltonian $H$ and $\Lambda(\mathbf{r} - \mathbf{r}')$ is a hydrodynamic kernel dependent upon the boundary conditions for the fluid medium in which the membrane resides. Additionally, we include a (Gaussian white) thermal random force $\zeta(\mathbf{r}', t)$ that satisfies the fluctuation−dissipation theorem[40]

$$\langle \zeta(\mathbf{r}, t) \rangle = 0$$

$$\langle \zeta(\mathbf{r}, t)\zeta(\mathbf{r}', t') \rangle = 2k_B T \Lambda^{-1}(\mathbf{r} - \mathbf{r}') \, \delta(t - t') \quad (3)$$

where the inverse of $\Lambda(\mathbf{r} - \mathbf{r}')$ is defined by

$$\int_{-\infty}^{\infty} d\mathbf{r}' \, \Lambda(\mathbf{r} - \mathbf{r}')\Lambda^{-1}(\mathbf{r}') = \delta(\mathbf{r}) \quad (4)$$

Although eq 2 is often quoted in the context of a membrane suspended in an infinite homogeneous hydrodynamic medium, the expression has generality beyond this case. It is this versatility that we exploit in this work. We shall present $\Lambda(\mathbf{r})$ for different boundary conditions corresponding to various physical situations in the next section.

The above equations for the membrane are most easily handled using Fourier modes defined by

$$h_{\mathbf{k}} = \int_A d\mathbf{r} \, h(\mathbf{r}) \, e^{-i\mathbf{k}\cdot\mathbf{r}} \quad (5)$$

$$h(\mathbf{r}) = \frac{1}{L^2} \sum_{\mathbf{k}} h_{\mathbf{k}} \, e^{i\mathbf{k}\cdot\mathbf{r}}$$

In Fourier space, the random force obeys[24]

$$\langle \zeta_{\mathbf{k}}(t) \rangle = 0$$

$$\langle \zeta_{\mathbf{k}}(t)\zeta_{\mathbf{k}'}(t') \rangle = 2k_B T L^2 \, \Lambda_{\mathbf{k}}^{-1} \, \delta_{\mathbf{k},-\mathbf{k}'} \, \delta(t - t') \quad (6)$$

The convenience of using the amplitudes $h_{\mathbf{k}}$ as dynamical variables is illustrated in the case where there are no additional interactions, $\mathscr{H}_{\text{int}} = 0$. All modes conveniently decouple, and eqs 1 and 2 simplify to

$$H = \frac{1}{2L^2} \sum_{\mathbf{k}} (\kappa k^4 + \sigma k^2) |h_{\mathbf{k}}|^2 \quad (7)$$

$$\frac{\partial h_{\mathbf{k}}(t)}{\partial t} = -\omega_{\mathbf{k}} h_{\mathbf{k}} + \Lambda_{\mathbf{k}} \zeta_{\mathbf{k}} \quad (8)$$

where we define the frequencies

$$\omega_{\mathbf{k}} \equiv \Lambda_{\mathbf{k}}(\kappa k^4 + \sigma k^2) \quad (9)$$

These equations describe an Ornstein-Uhlenbeck process[41] for each mode $h_{\mathbf{k}}$ whose known analytical solutions lead to the time correlation functions

$$\langle h_{\mathbf{k}}(t) h_{\mathbf{k}'}(0) \rangle = \frac{k_B T L^2}{\kappa k^4 + \sigma k^2} \, e^{-\omega_{\mathbf{k}} t} \, \delta_{\mathbf{k},-\mathbf{k}'} \quad (10)$$

$$\langle h(\mathbf{r}, t) h(\mathbf{r}, 0) \rangle = \frac{k_B T}{L^2} \sum_{\mathbf{k}} \frac{1}{\kappa k^4 + \sigma k^2} \, e^{-\omega_{\mathbf{k}} t} \quad (11)$$

In the general case where $\mathscr{H}_{\text{int}} \neq 0$, working in Fourier space is still useful for removing the convolution in eq 2

$$\frac{\partial h_{\mathbf{k}}(t)}{\partial t} = \Lambda_{\mathbf{k}}\{F_{\mathbf{k}}[h(\mathbf{r}, t)] + \zeta_{\mathbf{k}}(t)\} \tag{12}$$

The force $F_{\mathbf{k}}$ is a functional of the height field $h(\mathbf{r}, t)$ and, in general, depends on the entire set of amplitudes $\{h_{\mathbf{k}}\}$. In the case of harmonic interactions, it is possible to identify normal modes for the system, which still allows for analytical calculations and/or simplified simulations. Anharmonic potentials require a true simulation approach. We discuss both harmonic and anharmonic perturbations in the following sections. Before proceeding, however, the hydrodynamic kernel must be derived for the physical boundary conditions appropriate for the system. In the next section, we specify $\Lambda_{\mathbf{k}}$ for two different cases of interest.

## III. Hydrodynamic Kernels

This section presents a brief motivation for the hydrodynamic kernels adopted in the following calculations (eqs 22, 24, and 26−29). Further elaboration on the calculation of these quantities may be found in the original papers by Seifert[35] and Gov et al.[36]

The effect of surrounding fluid flow on membrane motion is determined by the Navier−Stokes equations for an incompressible fluid. In cellular environments, the Reynolds number is small,[39] and inertia can be neglected so that (Stokes equations[42])

$$\eta\nabla^2\mathbf{v} = \nabla p \tag{13}$$

where $\mathbf{v}$ is the velocity of the fluid with viscosity $\eta$, and $p$ is the pressure. Additionally, the incompressibility of the fluid requires that

$$\nabla\cdot\mathbf{v} = 0 \tag{14}$$

Boundary conditions for the system determine the solution for the velocity and pressure due to a given deformation of the membrane. In this work, the two cases of interest are that of a membrane in an infinite fluid and a membrane near an impermeable wall. Similar solutions for a membrane next to a permeable wall may also be derived[36] but will not be discussed here.

By performing the Fourier transform (in the $x$ and $y$ dimensions only as in eq 5) on the Navier−Stokes equations and the incompressibility condition, we derive the differential equation that $(v_z)_{\mathbf{k}}$ obeys

$$\partial_z^2[(-k^2 + \partial_z^2)(v_z)_{\mathbf{k}}] = k^2[(-k^2 + \partial_z^2)(v_z)_{\mathbf{k}}] \tag{15}$$

This equation can be reduced to

$$(-k^2 + \partial_z^2)(v_z)_{\mathbf{k}} = c_1' \sinh kz + c_2' \cosh kz \tag{16}$$

where the $c_i'$ are arbitrary constants. This second order differential equation has the solution

$$(v_z)_{\mathbf{k}} = c_1 \sinh kz + c_2 \cosh kz + c_3 z \sinh kz + c_4 z \cosh kz \tag{17}$$

All of the $c_i$ are arbitrary constants to be determined by the boundary conditions, which we specify below.

Taking the bilayer to be located at $z = 0$, the hydrodynamic kernel $\Lambda_{\mathbf{k}}$ can be derived from the requirement that the velocity of the fluid immediately adjacent to the membrane matches the velocity of the bilayer. This condition, expressed as $v_z^{\pm}(z = 0) = v_m$, combined with eq 12 leads to an equation involving the hydrodynamic kernel

$$[(v_z^{\pm})_{\mathbf{k}}]_{z=0} = \Lambda_{\mathbf{k}} F_{\mathbf{k}} \tag{18}$$

The superscript $\pm$ refers to the two fluid regions separated by the bilayer, the upper portion (+) and the lower portion (−). Defining the stress tensor for both upper and lower regions

$$T_{ij}^{\pm} \equiv \eta(\partial_i v_j^{\pm} + \partial_j v_i^{\pm}) - p^{\pm}\delta_{ij} \tag{19}$$

force balance between hydrodynamic stress and force on the bilayer implies

$$F_{\mathbf{k}} = [(T_{zz}^{-})_{\mathbf{k}} - (T_{zz}^{+})_{\mathbf{k}}]_{z=0} \tag{20}$$

The hydrodynamic kernel is therefore given by

$$\Lambda_{\mathbf{k}} = \left.\frac{(v_z)_{\mathbf{k}}}{(T_{zz}^{-})_{\mathbf{k}} - (T_{zz}^{+})_{\mathbf{k}}}\right|_{z=0} \tag{21}$$

where the velocity, the pressure, and the stress tensor are found by using eq 17 for a given set of boundary conditions.

We now specify the necessary boundary conditions for the cases considered in this work. For regions of fluid extending infinitely far away from the membrane, it must be the case that $\mathbf{v}(z) = 0$ at distances far from the membrane surface. The bilayer defines the other boundary for such a semi-infinite region. Continuity requires that the velocities of the fluid on either side of the membrane match at $z = 0$. This condition is expressed as $\mathbf{v}^+(z = 0) = \mathbf{v}^-(z = 0)$, where $\mathbf{v}^+$ and $\mathbf{v}^-$ are the solutions above and below the membrane, respectively. Additionally, a membrane with infinite regions of fluid on both sides is required by symmetry to respect $v_z^+(z) = v_z^-(-z)$. This condition leads to the solution

$$\Lambda_{\mathbf{k}}^{\text{inf}} = \frac{1}{4\eta k} \tag{22}$$

Our main interest is that of a membrane near an impermeable wall, which we take to be located at $z = -d$. The wall imposes the boundary condition $\mathbf{v}^-(z = -d) = 0$, which forces the velocity of the fluid to vanish there. To uniquely determine $\Lambda_{\mathbf{k}}$, an additional boundary condition must be specified at the membrane surface. Seifert[35] has argued for in-plane incompressibility of the membrane

$$[\partial_x v_x + \partial_y v_y]_{z=0} = 0 \tag{23}$$

which results in a solution

$$\Lambda_{\mathbf{k}}^{\text{S}} = \Lambda_{\mathbf{k}}^{\text{inf}} \frac{e^{2kd} + e^{-2kd} - 2[1 + 2(kd)^2]}{e^{2kd} - [1 + 2(kd)^2] + 2kd} \tag{24}$$

More recently, Gov et al.[36] have argued for boundary

conditions reflecting the fact that a fluid membrane is not expected to support shear stress. Mathematically, this translates to

$$[T_{xz}^{+} - T_{xz}^{-}]_{z=0} = 0 \tag{25}$$

(and similarly for $T_{yz}$) so that the shear stress is the same on both sides at the membrane. A different solution is found in this case

$$\Lambda_{\mathbf{k}}^{\mathrm{G}} = \Lambda_{\mathbf{k}}^{\mathrm{inf}}\, e^{-2kd}\{e^{2kd} - [\,1 + 2(kd\,)^2] - 2kd\} \tag{26}$$

Both solutions approach $\Lambda_{\mathbf{k}}^{\mathrm{inf}}$ as $kd$ becomes large, as expected on physical grounds. The hydrodynamics should be unaffected by the wall if the wall is far enough away (the magnitude of "far enough" is seen to depend on the wavelength of the deformation). However, as $kd$ becomes small, the limiting behavior of the two solutions differ by a factor of 4 such that $\Lambda_{\mathbf{k}}^{\mathrm{S}} \rightarrow k^2d^3/12\eta$ and $\Lambda_{\mathbf{k}}^{\mathrm{G}} \rightarrow k^2d^3/3\eta$. Using eq 9 for the noninteracting membrane as an approximate guide, we see that, in this limit, the relaxation times are longer for the scenario of Seifert.

We discuss the case of finding $\Lambda_{\mathbf{k}}$ when the viscosities above and below the membrane are different. The procedure for finding these solutions is similar to the one outlined already in this section. For notational convenience, we define $\bar{\eta} = (\eta^{+} + \eta^{-})/2$, $\xi^{\pm} = \eta^{\pm}/\bar{\eta}$, and $\Delta = (\eta^{+} - \eta^{-})/2\bar{\eta}$. The wall is located below the membrane where the viscosity is $\eta^{-}$. The solution for the membrane in the unbound fluid is

$$\Lambda_{\mathbf{k}}^{\mathrm{inf,general}} = \frac{1}{4\bar{\eta}k} \tag{27}$$

In the presence of the wall, the solution with Seifert's boundary condition is

$$\Lambda_{\mathbf{k}}^{\mathrm{S,general}} = \Lambda_{\mathbf{k}}^{\mathrm{inf,general}}\, \frac{e^{2kd} + e^{-2kd} - 2\,[1 + 2(kd)^2]}{e^{2kd} - [1 + 2(kd)^2]\xi^{+} + 2kd\xi^{-} + \Delta\, e^{-2kd}} \tag{28}$$

while the solution for Gov's boundary condition is

$$\Lambda_{\mathbf{k}}^{\mathrm{G,general}} = \Lambda_{\mathbf{k}}^{\mathrm{inf,general}}\, \frac{e^{-2kd}\,\{e^{2kd} - [1 + 2(kd)^2]\,\xi^{+} - 2kd\xi^{-}\} + \Delta\, e^{-4kd}}{1 - 2\Delta\, e^{-2kd}[1 + 2(kd)^2] + \Delta^2 e^{-4kd}} \tag{29}$$

In the case of $\eta^{+} = \eta^{-}$, $\xi^{\pm} = 1$ and $\Delta = 0$, and we recover the solutions in eqs 22, 24, and 26.

The general effect of the wall is to slow the relaxation of the membrane. The confinement of water between the membrane surface and the adjacent wall hinders relaxation of the membrane. For an estimate of the difference between the decay times of a bound and unbound fluid, we refer, again, to eq 9 for the noninteracting membrane. Since the relaxation time of the amplitude $h_{\mathbf{k}}$ is given by $1/\omega_{\mathbf{k}}$, we see that the presence of the wall slows the membrane by a factor of $\sim 1/(kd)^3$ in the limit of small $kd$. The dynamics of the membrane can be altered significantly if the wall is close enough to the bilayer or if the dominant modes have a sufficiently long wavelength.

## IV. Independent Modes

Since we work with the amplitudes $h_{\mathbf{k}}$ as the dynamical variables, it is important to recognize that they are not all independent (even if $\mathscr{H}_{int} = 0$). Since $h(\mathbf{r})$ is a real quantity, the amplitudes must obey condition $h_{\mathbf{k}}^{*} = h_{-\mathbf{k}}$. In addition, we generally discretize $h(\mathbf{r})$ to avoid handling an infinite number of modes and to coarse-grain over microscopic details. Let the height field be discretized as an $N \times N$ matrix with a lattice spacing $\ell = L/N$ so that the allowed wave vectors are $\mathbf{k} = (m, n)2\pi/L$ with $-N/2 < m, n \leq N/2$. To proceed with any calculations or simulations, it is first necessary to find $N^2$ independent variables with which to work.

The discrete Fourier transform of a real $N \times N$ matrix has four explicitly real modes if $N$ is even, and one explicitly real mode if $N$ is odd. We consider only the case where $N$ is even (the procedure for odd $N$ follows in a straightforward fashion). The explicitly real modes are $(m, n) = (0, 0)$, $(N/2, 0)$, $(0, N/2)$, and $(N/2, N/2)$. Note that the center of mass $h_{\mathrm{cm}}$ is related to the $(m, n) = (0, 0)$ mode by the equation

$$h_{\mathrm{cm}} = \frac{h_{\mathbf{k}=0}}{L^2} \tag{30}$$

(In this work we always consider systems with a fixed center of mass and the $(m, n) = (0, 0)$ mode is not considered a dynamical variable.) We label the remaining three explicitly real modes as $\mathbf{q}_r$: $(m, n) = (N/2, 0)$, $(0, N/2)$, and $(N/2, N/2)$. The remaining independent modes are chosen based on the condition $h_{\mathbf{k}}^{*} = h_{-\mathbf{k}}$. We label these $N^2/2-2$ modes $\mathbf{q}_c$: $(m, n)$ for $-N/2 < m < N/2$ and $0 < n < N/2$, $(m, 0)$ for $0 < m < N/2$, $(m, N/2)$ for $0 < m < N/2$, and $(N/2, n)$ for $0 < n < N/2$. These modes are illustrated graphically in Figure 1.

Defining the real and imaginary parts of the amplitudes to be $h_{\mathbf{k}} \equiv a_{\mathbf{k}} + ib_{\mathbf{k}}$, the set of $N^2$ independent modes can be listed as $(\{a_{\mathbf{q}_c}\},\{a_{\mathbf{q}_r}\},\{b_{\mathbf{q}_c}\})$. We define a vector of length $N^2 - 1$

$$\mathbf{q} \equiv (\{\mathbf{q}_c^{\mathrm{real}}\}, \{\mathbf{q}_r\}, \{\mathbf{q}_c^{\mathrm{imag}}\}) \tag{31}$$

as a way of indexing these independent modes. Although the sets $\{\mathbf{q}_c^{\mathrm{real}}\}$ and $\{\mathbf{q}_c^{\mathrm{imag}}\}$ both span the same values as $\{\mathbf{q}_c\}$, the superscript labels are used for clarity. Note that $\mathbf{k}$ is the Fourier index, while $\mathbf{q}$ is just a vector for the independent modes defined by eq 31.

All of the above also applies to $\zeta(\mathbf{r})$. Defining $\xi_{\mathbf{k}} \equiv f_{\mathbf{k}} + ig_{\mathbf{k}}$, the set of independent random forces is $(\{f_{\mathbf{q}_c}\},\{f_{\mathbf{q}_r}\},\{g_{\mathbf{q}_c}\})$. Using eq 6, the fluctuation−dissipation relations become

$$\langle\, f_{\mathbf{q}_c}(t)\rangle = \langle\, f_{\mathbf{q}_r}(t)\rangle = \langle g_{\mathbf{q}_c}(t)\rangle = 0$$

$$\langle\, f_{\mathbf{q}_c}(t) f_{\mathbf{q}_c}(t')\rangle = \langle g_{\mathbf{q}_c}(t) g_{\mathbf{q}_c}(t')\rangle = k_B T L^2 \Lambda_{\mathbf{q}_c}^{-1}\delta(t - t')$$

$$\langle\, f_{\mathbf{q}_r}(t) f_{\mathbf{q}_r}(t')\rangle = 2k_B T L^2 \Lambda_{\mathbf{q}_r}^{-1}\delta(t - t') \tag{32}$$

All cross correlations are equal to zero.

## V. Harmonic Interactions

We focus on a physical situation for which a harmonic form of the interaction potential is appropriate. Specifically, we

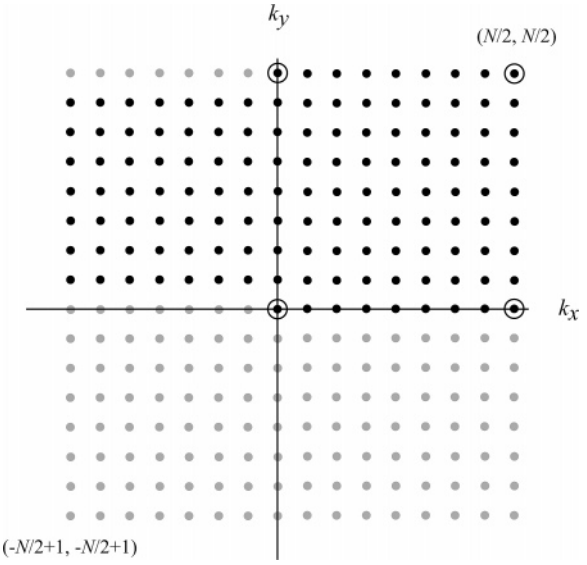


***Figure 1.*** Plot of the $N^2$ modes (for $N$ even) in **k** space. The four circled, black dots are the real modes consisting of the center of mass mode, $\mathbf{k} = 0$, and the other three modes $\{\mathbf{q}_r\}$. The remaining black dots are the independent, complex modes $\{\mathbf{q}_c\}$, while the gray dots are the dependent, complex conjugates of $\{\mathbf{q}_c\}$. Each $\mathbf{q}_r$ contributes one independent variable, while each $\mathbf{q}_c$ contributes two independent variables. The ($m$, $n$) values for the upper-right and lower-left modes are shown in the plot to define the boundaries in $k_x$ and $k_y$ space.

are interested in interactions that strongly bind the bilayer to a height of $z_i$ at localized positions $\mathbf{R}_i$ in the plane of membrane. Such a pinning interaction is described by the equation

$$\mathcal{H}_{\text{pin}}[h(\mathbf{r})] = \frac{\gamma}{2}\sum_i [h(\mathbf{r}) - z_i]^2 \delta(\mathbf{r} - \mathbf{R}_i) \tag{33}$$

with a resulting force

$$F_{\text{pin}}(\mathbf{r}) = -\gamma \sum_i [h(\mathbf{r}) - z_i]\delta(\mathbf{r} - \mathbf{R}_i) \tag{34}$$

We discuss here and in the Appendix a method for obtaining averages and time correlation functions without the need for simulations. The procedure described here is an extension of previous work.[32] In Fourier space, the full set of equations can be written as

$$H = \frac{1}{2L^2}\left(\sum_{\mathbf{k},\mathbf{k}'} h_{\mathbf{k}}^* M'_{\mathbf{k}\mathbf{k}'} h_{\mathbf{k}'} + 2\sum_{\mathbf{k}} m'_{\mathbf{k}} h_{\mathbf{k}}\right)$$

$$\frac{\partial h_{\mathbf{k}}(t)}{\partial t} = \Lambda_{\mathbf{k}}\left(-\sum_{\mathbf{k}'} M'_{\mathbf{k}\mathbf{k}'} h_{\mathbf{k}'}(t) - m'_{\mathbf{k}} + \zeta_{\mathbf{k}}(t)\right) \tag{35}$$

where

$$M'_{\mathbf{k}\mathbf{k}'} = (\kappa k^4 + \sigma k^2)\delta_{\mathbf{k},\mathbf{k}'} + \frac{\gamma}{L^2}\sum_i e^{-i(\mathbf{k}-\mathbf{k}')\cdot\mathbf{R}_i}$$

$$m'_{\mathbf{k}} = \gamma \sum_i (h_{\text{cm}} - z_i)\, e^{i\mathbf{k}\cdot\mathbf{R}_i} \tag{36}$$

and the sums exclude $\mathbf{k} = 0$. In this work, we are interested exclusively in systems with a fixed center of mass

$$h_{\text{cm}} = \frac{h_{\mathbf{k}=0}}{L^2} \tag{37}$$

which appears explicitly as a constant in $m'_{\mathbf{k}}$.

Since the modes in the above equations are mixed, we use matrix diagonalization to decouple the amplitudes $h_{\mathbf{k}}$. This procedure is somewhat complicated and is relegated to the Appendix. After diagonalization, the equations can be written in terms of the eigenmodes $d_j$, the eigenvalues $\omega_j$, and the orthogonal transformation matrix **U**. The completely decoupled equations are

$$H = \frac{1}{L^2}\sum_j (\omega_j d_j^2 + 2n_j d_j) \tag{38}$$

$$\frac{\partial d_j(t)}{\partial t} = -\omega_j d_j(t) - n_j + s_j(t) \tag{39}$$

where $n_j$ is a time-independent constant defined in the Appendix. The quantities $s_j(t)$ is related to the original random forces in eq 6 and obey the fluctuation−dissipation relations

$$\langle s_j(t)\rangle = 0$$

$$\langle s_j(t)s_j(t')\rangle = k_B T L^2 \delta(t - t') \tag{40}$$

The above equations define a set of independent Ornstein-Uhlenbeck processes[41] for the evolution of the harmonically pinned membrane surface. As such, it is a simple matter to simulate the stochastic behavior of the membrane by drawing random numbers from suitable Gaussian distributions. We do not pursue this type of simulation in the present work but instead calculate the average membrane shape, fluctuations, and dynamics analytically from the normal mode decomposition. Averages and time correlations for the eigenmodes $d_j$ can be calculated in a way similar to the case of the noninteracting membrane. The results are

$$\langle d_j\rangle = -\frac{n_j}{\omega_j} \tag{41}$$

$$\langle d_j^2\rangle = \frac{k_B T L^2}{2\omega_j} \tag{42}$$

$$\langle d_j(\text{t}) d_j(0)\rangle - \langle d_j\rangle^2 = \sigma_j^2\, e^{-\omega_j t} \tag{43}$$

where $\sigma_j^2 \equiv \langle d_j^2\rangle - \langle d_j\rangle^2$. The equations lead to the average height and time correlation functions

$$\langle h(\mathbf{r})\rangle = h_{\text{cm}} + \sum_j \upsilon_j(\mathbf{r})\,\langle d_j\rangle$$

$$\langle h(\mathbf{r}, t)h(\mathbf{r}, 0)\rangle - \langle h^2(\mathbf{r})\rangle = \sum_j \upsilon_j^2(\mathbf{r})\,\sigma_j^2\, e^{-\omega_j t} \tag{44}$$

where $\upsilon_j(\mathbf{r})$ is defined in the Appendix.

## VI. Nonharmonic Interactions

We now discuss the more general case in which the physical interaction cannot be written in terms of a harmonic potential.

In this situation, a simulation must, in general, be performed. We describe a Fourier Space Brownian Dynamics (FSBD) method[33,34] for time evolving the membrane based on standard Brownian dynamics.[43] The essential difference between the two methods is that, rather than using the position space variables, the amplitudes $h_{\mathbf{k}}$ are evolved instead. By making this choice, the computationally expensive convolution in eq 2 is avoided.

We first integrate eq 12 from $t$ to $t + \Delta t$ for small $\Delta t$ to get

$$h_{\mathbf{k}}(t + \Delta t) = h_{\mathbf{k}}(t) + \Lambda_{\mathbf{k}} F_{\mathbf{k}}(t)\Delta t + \Gamma_{\mathbf{k}}(\Delta t)$$

$$\Gamma_{\mathbf{k}}(\Delta t) \equiv \Lambda_{\mathbf{k}} \int_t^{t+\Delta t} dt'\, \zeta_{\mathbf{k}}(t') \tag{45}$$

Exactly $N^2$ independent random values must be chosen to properly construct $\Gamma_{\mathbf{k}}(\Delta t)$. We therefore restrict ourselves to the modes $\mathbf{q}$ defined eq 31. Using eq 32, it can be shown that the real and imaginary parts of $\Gamma_{\mathbf{q}_c}(\Delta t)$ are both drawn from a Gaussian distribution of mean zero and variance $k_B T L^2 \Lambda_{\mathbf{k}} \Delta t$, while $\Gamma_{\mathbf{q}_r}(\Delta t)$ is drawn from Gaussian distribution of mean zero and variance $2k_B T L^2 \Lambda_{\mathbf{k}} \Delta t$. After picking random values for $\Gamma_{\mathbf{q}}(\Delta t)$, the full matrix for $\Gamma_{\mathbf{k}}(\Delta t)$ can then be reconstructed.

The FSBD method is summarized below:

1. Evaluate the interaction part of the forces $F_{\text{int}}(\mathbf{r}) = -\delta \mathscr{H}_{\text{int}}/\delta h(\mathbf{r})$ in position space.

2. Compute the bending forces $-\kappa k^4 h_{\mathbf{k}}$ and surface tension forces $-\sigma k^2 h_{\mathbf{k}}$. Evaluate the interaction force $F_{\mathbf{k}}^{\text{int}}$ by Fourier transforming the result of the previous step.

3. As described above, draw random values from the appropriate Gaussian distributions for the independent modes only. Construct $\Gamma_{\mathbf{k}}(\Delta t)$ from these values.

4. Compute $h_{\mathbf{k}}(t + \Delta t)$ using eq 45. Inverse Fourier transform $h_{\mathbf{k}}$ to obtain $h(\mathbf{r})$ for use in the next iteration.

It is essential to choose a sufficiently small time step $\Delta t$ such that the results have converged.

## VII. Application of Harmonic Dynamics: Fluctuation Time Scales for Intermembrane Junctions

Lipid bilayers supported by solid substrates have become important tools for studying various membrane-related biophysical processes.[44] These bilayers are either directly fixed to the surface or are separated from the substrate by a thin layer of water or a polymer cushion. Membranes that are not directly attached to the surface retain their fluid properties,[45] making them useful as model systems for studying processes, such as the formation of the immunological synapse,[46,47] that involve the free diffusion of components in the bilayer.

In this section, we focus on a recent experimental study of supported intermembrane junctions by Kaizuka and Groves.[37] In these experiments, giant unilamellar vesicles were ruptured over a previously deposited planar supported membrane surface. The ruptured vesicles were observed to adhere to the underlying supported bilayer in two distinct fashions (see Figure 2). Either the two bilayers adhere to one another with a nearly uniform separation of a few nanometers ("Type 1" intermembrane junction), or the two bilayers form an irregular interface with average separation on the order of 50 nanometers held together by a sparse randomly distributed network of pinning sites where the two bilayers closely approach one another ("Type 2" intermembrane junction). In the Type 2 junctions, an appreciable volume of water is effectively trapped between upper and lower bilayers, making these systems a natural realization of hydrodynamic flow next to an impermeable wall. The reason for the formation of these distinct structures and the nature of the localized pinning in the Type 2 systems remain poorly understood. Kaizuka and Groves[37] have studied the average height and dynamic fluctuations of Type 2 junctions via fluorescence interference contrast (FLIC) microscopy,[48,49] and it is these data that we discuss here.

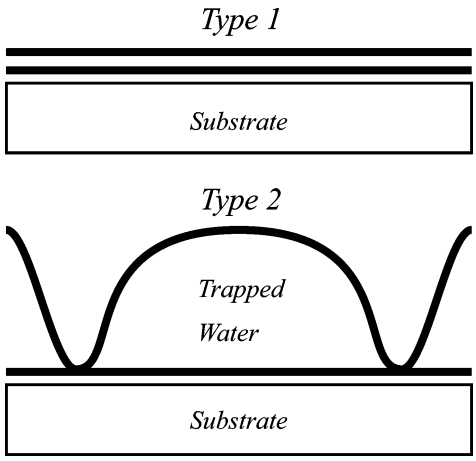


***Figure 2.*** Illustration of the two types of junctions (adapted from ref 37). The thick line on the bottom and directly over the substrate represents the supported lipid bilayer. The giant unilamellar vesicle that has been ruptured over this planar bilayer is represented by another thick line above it. Type 1 junctions have intermembrane spacings of about 2−3 nm compared to Type 2 junctions which can have spacings of about 50 nm as well as localized adhesion sites.

We model this system by assuming that the upper membrane surface is locally pinned to the supported bilayer in a geometry directly inferred from experimental data—we make no attempt to account for the physical basis of this random adhesion. This localized pinning is achieved by using the potential in eq 33 with $\gamma$ sufficiently large to fix the membrane at height $z_i = 0$ at the experimentally determined pinning sites $\mathbf{R}_i$ (i.e. we define the height of the upper bilayer to be zero ($h(\mathbf{R}_i) = 0$) where the pinning occurs). For the purposes of this simulation, the lower bilayer is an impermeable wall located at $z = 0$. The system size $L = N\ell \sim 5.4$ $\mu$m, with $N = 64$ and $\ell \sim 85$ nm correspond with the size and resolution obtained in experiment. We account for the trapped volume of water in the junction by setting $h_{\text{cm}}$ to a positive constant value. This is equivalent to a constant volume condition for our periodic boundary condition simulations. The distance $d$ of the membrane from the wall in the expression for $\Lambda_{\mathbf{k}}$ is therefore set equal to $h_{\text{cm}}$. We also assume that the interactions responsible for pinning the membrane to the supported bilayer dictate the slope of the membrane around the pin. To model this boundary condition

***Table 1.*** Model Parameters for the Intermembrane Junction

| parameter | description | value | reference |
|---|---|---|---|
| $\kappa$ | bending modulus | $7 \times 10^{-12}$ ergs | *a* |
| $\sigma$ | surface tension | 0.08 dyn/cm | *b* |
| $\eta$ | viscosity | 0.01 poise | water |
| $T$ | temperature | 20 °C | *c* |
| $L$ | system size | 5.4 $\mu$m | *d* |
| $l$ | lattice spacing | 85 nm | *d* |
| $s$ | slope around pinned site | 0.29 | *b* |
| $h_{cm}$ | center of mass | 46 cm | *b* |
| $\gamma$ | pinning constant | $10^8$ ergs cm$^{-2}$ | *e* |

[a] Personal communication with Kaizuka and Groves.[37] [b] Fit to data of ref 37. [c] Reference 37. [d] From data provided by ref 37. [e] Sufficiently large to fix the membrane at the pinning site. Simulations with larger values of $\gamma$ give identical results.

within our harmonic scheme, we harmonically bind the four sites immediately adjacent to the pin location at a height of $z_i = h_n$ using eq 33, which leads to a slope $s = h_n/\ell$. The average shape of the junction and magnitude of fluctuations can then be calculated using eq 44 assuming the experimental conditions of $T = 293$ K and $\eta = 0.01$ poise and implementing either of the two hydrodynamic kernels previously discussed.

The values chosen for the physical parameters $h_{cm}$, $s$, $\kappa$, and $\sigma$ must be obtained by fitting to the experimental data, a process significantly complicated by the limited lateral resolution of the FLIC technique (i.e. the experimental data reflects a convolution in space over the point spread function of the laser). The procedure involved is beyond the scope of this work, so we simply quote the results for our parameters in Table 1. A detailed account of the agreement between experiment and theory for the average shape and fluctuations of the junction will be presented elsewhere.[50] The present work is concerned with the impact of different hydrodynamic kernels on relaxation time scales, and we focus on this question here. To give an idea of the shapes generated by these simple elastic considerations we do present the shape and fluctuations for a representative arrangement of pinning sites (Figure 3).

Time correlation functions for height fluctuations in this system have been measured experimentally with observed decay times in the range of hundreds of milliseconds to seconds[38] depending on the particular junction probed and the location of the observed fluctuation within the pinned geometry. Since the supported planar bilayer should act as an impermeable boundary to fluid flow, the hydrodynamic kernels in eqs 24 and/or 26 are expected to apply.

In Figure 4, we plot the predicted time correlation function at several locations distributed over the membrane surface and using both suggested hydrodynamic kernels. Our results show relaxation times in qualitative agreement with experimental results. The difference between results employing Seifert's and Gov's hydrodynamic boundary conditions are appreciable but not so striking as to rule one form out in favor of the other on the basis of available experimental data. What is clear is that the inclusion of the impermeable wall in some fashion is necessary to set relaxation time scales close to experimental values. Blindly applying the standard result in eq 22 for a membrane in an infinite fluid medium leads to relaxation times orders of magnitude too fast relative to experiment.

For comparison, we also plot the results without hydrodynamics by using a constant value $\Lambda_{\mathbf{k}} = 1/4\eta k_0$ for all $\mathbf{k}$, where $k_0 = 2\pi/L$ is the longest wavelength mode in the system. The choice of this constant value ensures that the longest wavelength mode evolves as it would with hydrodynamics. The other modes, however, evolve with a kernel that is $k/k_0$ times larger than the hydrodynamical value. For concreteness and simplicity, we first study the relaxation frequencies of the membrane without interactions in eq 9. The decay time for each mode is proportional to $1/\Lambda_{\mathbf{k}}$ so that the shorter wavelength modes have shorter decay times when the constant value of $1/4\eta k_0$ is used. This analysis should also be approximately true in the case where there are interactions. The effect of faster decay by the shorter wavelength modes can be seen over the shorter times scales in Figure 4.

The time scales seen in our figures are in general agreement with a more simplified approach to analyzing the

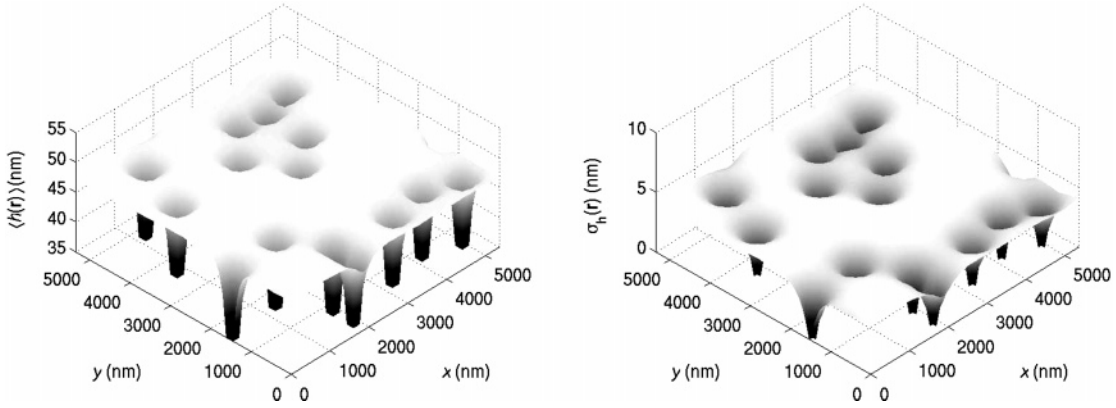


***Figure 3.*** Average bilayer shape and fluctuations for a representative configuration of pinning sites in a Type 2 intermembrane junction. The results were obtained using the diagonalization procedure of section V with the physical constants listed in Table 1. The left panel shows the results for the average height $\langle h(\mathbf{r})\rangle$. Note that the bottom of the wells are pinned at a height of 0 (outside the range of the plot). The right panel shows the size of the height fluctuations $\sigma_h(\mathbf{r}) \equiv \sqrt{\langle h^2(\mathbf{r})\rangle - \langle h(\mathbf{r})\rangle^2}$. Both left and right panels display the data with $z$ axis significantly expanded relative to $x$, $y$ to show detail.

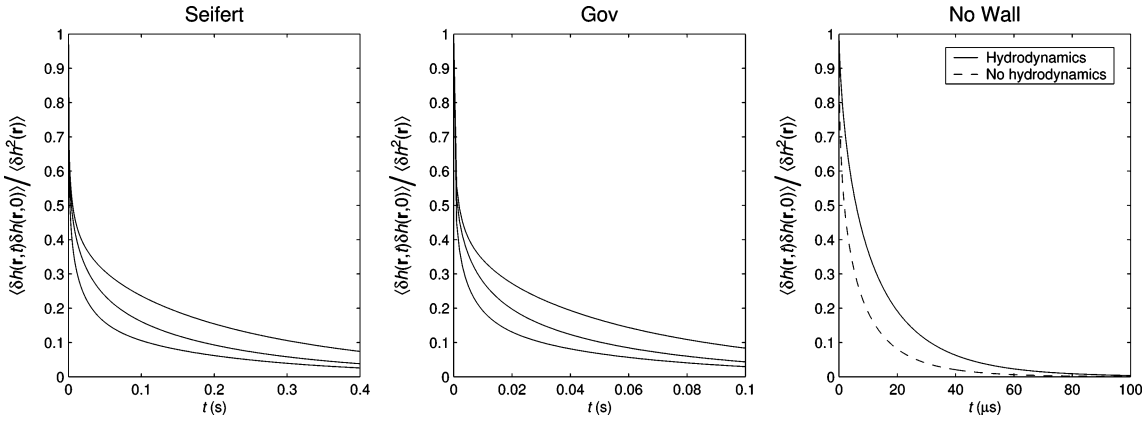


***Figure 4.*** Plot of typical time correlations functions $\langle \delta h(\mathbf{r}, t)\delta h(\mathbf{r}, 0)\rangle$, where $\delta h(\mathbf{r}, t) \equiv h(\mathbf{r}, t) - \langle h(\mathbf{r})\rangle$, for different boundary conditions. The results are shown for Seifert's boundary condition in the left panel and Gov's boundary condition in the middle panel. The three curves indicate roughly the range of decay times for different locations on the membrane away from the pinning sites. In the right panel, a typical correlation function for a hydrodynamic kernel assuming an infinite fluid environment (no wall) is shown. For comparison, results without hydrodynamics are also plotted. In that case, we use a constant value $\Lambda_{\mathbf{k}} = 1/4\eta k_0$, where $k_0 = 2\pi/L$ is the longest wavelength mode in the system. The time scales for relaxation when there is no wall are orders of magnitude faster than the observed experimental decay times of hundreds of milliseconds to seconds.[38] Incorporation of the proper hydrodynamic kernel is necessary to model the experiment.

data suggested by Kaizuka and Groves.[38] In that work, Gov's form for the hydrodynamic kernel was employed, but an empirical Hamiltonian was introduced to constrain the upper membrane at a fixed height from the support. As far as the dynamics are concerned, the two methods produce similar results. The present study has the advantage of fitting all available experimental data to an elastic model that is physically motivated (albeit with an unexplained pinning interaction). We stress that the difference between the predicted relaxation rates for the $\Lambda_{\mathbf{k}}$ with and without the wall is several orders of magnitude. The presence of a wall slows the dynamics of the membrane significantly and must be included for proper modeling of experiment.

## VIII. Application of Anharmonic Dynamics: Red Blood Cell Protein Mobility

In previous work,[33,34,51] we have studied the effect of thermal membrane undulations on the lateral diffusivity of band 3 protein over the surface of the red blood cell. Band 3 is known to diffuse freely over length scales less than ~100 nm, but its motion is hindered over larger distances.[52−56] The reason for the slower diffusion on longer length scales is the presence of the cell's cytoskeleton, which consists of roughly triangular corrals formed by spectrin filaments[57,58] attached to the membrane in a quasi-regular geometry. The microscopic diffusion constant,[59] $D = 0.53\ \mu\text{m}^2\ \text{s}^{-1}$, on scales smaller than the size of the corrals,[59] $L_c \sim 110$ nm, is in good agreement with estimates for protein diffusivity in a viscous quasi-two-dimensional environment.[60] However the macroscopic diffusion constant, relevant over longer length scales, takes on a value, $D_{\text{macro}} = 6.6 \times 10^{-3}\ \mu\text{m}^2\ \text{s}^{-1}$, 2 orders of magnitude smaller.[59,61−66]

Although the cytoskeleton hinders protein motion, band 3 does manage to escape confinement as evidenced by the finite macroscopic diffusion coefficient. One possible mechanism for this escape process is that thermal membrane fluctuations may help the protein to escape local confinement by lifting the cytoplasmic domain of the protein over the top of the cytoskeletal barriers.[33,34,51] Using methods similar to those of our prior studies, we calculate the expected $D_{\text{macro}}$ resultant from fluctuations in bilayer shape. In contrast to previous work we include in this study a hydrodynamic kernel that approximately accounts for the hampered flow of cytoplasm (and hence slowed motion of the bilayer) due to the presence of spectrin filaments.

We model the interactions of the membrane with the cytoskeleton with a combination of two potentials. First, the bilayer is pinned to the membrane at discrete points using eq 33 to mimic the attachment of the membrane to the spectrin filaments. Second, the steric interaction between the membrane and the cytoskeleton is modeled with the repulsive hydration potential[67]

$$\mathscr{H}_{\text{rep}}[h(\mathbf{r})] = \epsilon\, e^{-h(\mathbf{r})/\lambda} \sum_i \exp\left\{-\left(\frac{a_i x + b_i y + c_i}{\ell/4}\right)^2\right\} \qquad (46)$$

where $a_i x + b_i y + c_i = 0$ specifies a particular linear segment of spectrin between pinning sites. The repulsive interaction is localized to this set of lines with a width of about $\ell = 7$ nm. The physical parameters used for this system are shown in Table 2.

Since the repulsive interaction in eq 46 is not harmonic, we must perform a simulation of the membrane to compute averages of interest, as detailed in section VI. In Figures 5 and 6, we show sample configurations of two different geometries generated using the FSBD simulation method. Since altering the hydrodynamics of the system only affects dynamics and not thermal statistics, these configurations are consistent with what was seen in our prior studies without the inclusion of hydrodynamic effects imposed by spectrin (see below).

We develop a model of protein mobility that incorporates thermal fluctuations of the lipid bilayer. Band 3 protrudes into the cellular interior a distance of $h_0 = 6$ nm[69] and

**Table 2.** Model Parameters for the Red Blood Cell

| parameter | description | value | reference |
|---|---|---|---|
| $\kappa$ | bending modulus | $2 \times 10^{-13}$ ergs | *a* |
| $\sigma$ | surface tension | 0 | *b* |
| $\eta^+$ | water viscosity | 0.01 poise | water |
| $\eta^-$ | cytoplasm viscosity | 0.06 poise | *a* |
| $T$ | temperature | 37° C | body temp |
| $h_0$ | depth of cytoplasmic domain of band 3 | 6 nm | *c* |
| $D$ | band 3 diffusion constant | 0.53 $\mu$m$^2$ s$^{-1}$ | *d* |
| $L_c$ | corral size | 112 nm | *d*, *e* |
| $l$ | lattice spacing | 7 nm | *e* |
| $t_D$ | random walk time step | 23 $\mu$s | *e* |
| $\gamma$ | pinning constant | 100 ergs cm$^{-2}$ | *e* |
| $\epsilon$ | repulsive potential energy scale | $8.7 \times 10^{-4}$ ergs cm$^{-2}$ | *f* |
| $\lambda$ | repulsive potential length scale | 0.2 nm | *g* |

[a] Reference 23. [b] Reference 68. [c] Reference 69. [d] Reference 59. [e] Reference 32. [f] References 33 and 34. [g] Reference 67.

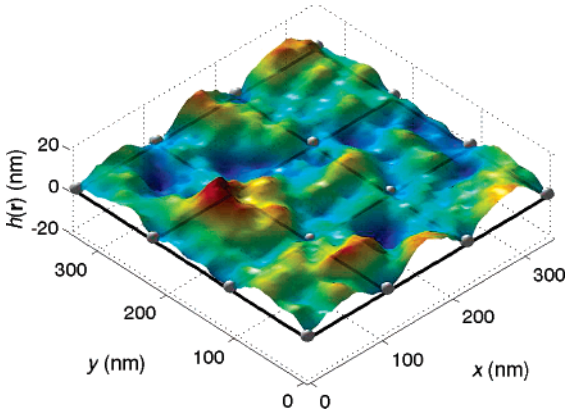


***Figure 5.*** Sample configuration for a membrane with square pinning and cytoskeletal repulsion. The pinning sites are indicated by spheres and the repulsive interaction due to spectrin is localized along the black lines which connect between the pinning sites. The *z*-axis is expanded to help visualize fluctuations in the membrane.

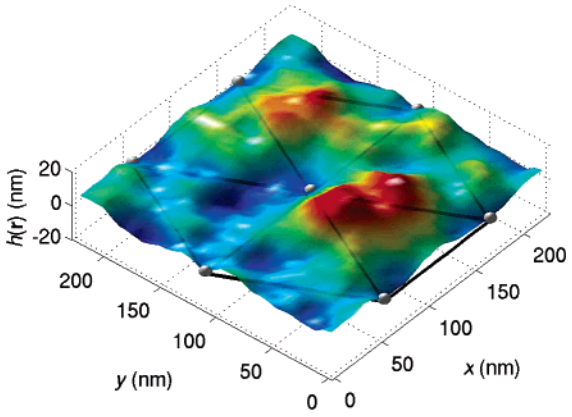


***Figure 6.*** The same plot as in Figure 5, except for a triangular geometry.

interacts sterically with the cytoskeleton as it diffuses within the corral. The first requirement for band 3 escape from the corral is that the separation between spectrin and bilayer locally exceed $h_0$, so that there is a large enough gap for the protein to slip through. Second, the height fluctuation should persist long enough for the protein to diffuse a distance equal to the width of the spectrin filament (approximately $\ell = 7$ nm). On average, the time to diffuse this distance is $t_D = \ell^2/4D = 23\ \mu$s. An escape probability along the corral edge can be calculated by using FSBD to find correlated probability that $h(\mathbf{r}) > h_0$ at both times 0 and $t_D$. Knowledge of this escape probability leads to the macroscopic diffusion constant $D_{macro}$ as detailed in our previous studies.[33,34]

In previous work,[32−34,51] we assumed that the red blood cell membrane was fluctuating in an unbound fluid characterized by the viscosity of the red cell cytoplasm. In recent work by Gov et al.,[26] it was proposed that the cytoskeleton acts as a source of confinement of hydrodynamic flow. The use of the hydrodynamic kernel with a wall in eq 26 provided improved fits to experimental dynamic membrane fluctuation data relative to models incorporating infinite hydrodynamic boundaries. Since we choose to use the value $d = 35$ nm determined using the hydrodynamic kernel proposed by Gov et al.,[26] we use that version of the kernel (eqs 26 and 29) in our simulations.

We illustrate the effect of the wall by studying the probability that the membrane height lies above $h_0$ at time $t$ given that it was above $h_0$ at time 0 defined by

$$C(\mathbf{r}, t) = \frac{\langle \Theta(h(\mathbf{r}, t) - h_0)\Theta(h(\mathbf{r}, 0) - h_0)\rangle - P^2(\mathbf{r})}{P(\mathbf{r}) - P^2(\mathbf{r})} \qquad (47)$$

where $P(\mathbf{r})$ is the equilibrium probability that $h(\mathbf{r}) > h_0$ given by

$$P(\mathbf{r}) = \langle \Theta(h(\mathbf{r}) - h_0)\rangle \qquad (48)$$

and $\Theta$ is the Heaviside step function. The escape probability, and therefore $D_{macro}$, depends on the value of $P(\mathbf{r})C(\mathbf{r}, t_D)$. In Figure 7, we plot a comparison of $C(\mathbf{r}, t)$ for two different hydrodynamic kernels. As expected, the membrane relaxation is slowed in the presence of an impermeable wall.

Historically, we have calculated $D_{macro}$ using $P(\mathbf{r})C(\mathbf{r}, t_D)$ because analytical results are available for harmonic potentials. Using FSBD however, it is possible to calculate the probability that the membrane remain above $h_0$ for the entire time interval $t_D$, defined to be

$$P_{open}(\mathbf{r}, t) = \langle \delta(t_D - \int_0^{t_D} ds\ \Theta\ (h(\mathbf{r}, s) - h_0))\rangle \qquad (49)$$

In our case, we require that $h(\mathbf{r}, t) > h_0$ at each time step $\Delta t$

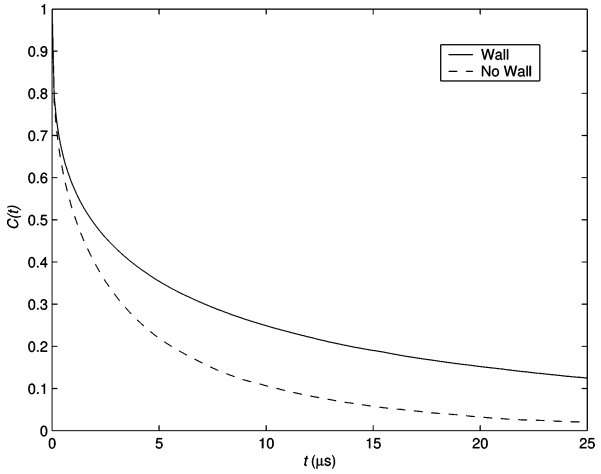


***Figure 7.*** Plot of $C(\mathbf{r}, t)$ in eq 47, the correlated probability that the membrane height is greater than $h_0$ at time $t$ given that it was greater than $h_0$ at time 0. The results shown are for the point $\mathbf{r} = (L_c/2, 0)$ in a square geometry. The relaxation of the membrane in the presence of the wall is slower than that of a membrane in an unbound fluid.

***Table 3.*** Results for $D_{\text{macro}}$ for Various Cases[a]

| | $1000D_{\text{macro}}$ ($\mu\text{m}^2\ \text{s}^{-1}$) using $P(\mathbf{r})C(\mathbf{r}, t_D)$ | $1000D_{\text{macro}}$ ($\mu\text{m}^2\ \text{s}^{-1}$) using $P_{\text{open}}(\mathbf{r}, t_D)$ |
|---|---|---|
| experiment | 6.6 | |
| square, $\eta^+ = \eta^-$, no wall | $37.8 \pm 2.0$ | $2.83 \pm 0.25$ |
| triangle, $\eta^+ = \eta^-$, no wall | $18.8 \pm 5.3$ | $2.02 \pm 0.38$ |
| square, $\eta^+ = \eta^-$, wall | $188 \pm 3$ | $20.3 \pm 1.2$ |
| triangle, $\eta^+ = \eta^-$, wall | $155 \pm 3$ | $18.0 \pm 0.9$ |
| square, $\eta^+ \neq \eta^-$, no wall | $7.40 \pm 1.7$ | $0.151 \pm 0.048$ |
| triangle, $\eta^+ \neq \eta^-$, no wall | $6.12 \pm 0.17$ | $0.0560 \pm 0.0283$ |
| square, $\eta^+ \neq \eta^-$, wall | $43.5 \pm 1.9$ | $0.859 \pm 0.102$ |
| triangle, $\eta^+ \neq \eta^-$, wall | $20.5 \pm 2.2$ | $0.490 \pm 0.105$ |

[a] The FSBD simulations were performed over a time of $t = 30$ ms using a time step of $\Delta t = 1$ ns. When the viscosities above and below the membrane are the same, we use the cytoplasmic viscosity $\eta = \eta^-$ (see Table 2) consistent with our prior work.[32−34,51]

in our simulation. It should be emphasized that, in the absence of detailed modeling of the interactions between the membrane, cytoskeleton, and protein, both $P(\mathbf{r})C(\mathbf{r}, t_D)$ or $P_{\text{open}}(\mathbf{r}, t)$ serve as approximations for the calculation of $D_{\text{macro}}$. It is not clear a priori which approximation should serve as a closer mimic to experiment.

The values of the macroscopic diffusion constant for various scenarios are shown in Table 3. We note several observations for the different scenarios listed. First, as a result of the increased temporal persistence of fluctuations due to the wall, the macroscopic diffusion constants are larger relative to the case of a membrane in an unbound fluid. Second, using the viscosity of water for $\eta^+$ so that $\eta^+ < \eta^-$ (a more realistic scenario for the case of a red blood cell in a biological environment) decreases the relaxation time for the membrane and therefore decreases $D_{\text{macro}}$. Finally, the use of $P_{\text{open}}(\mathbf{r}, t_D)$ is a more restrictive condition and decreases the macroscopic diffusion constant as compared to the value obtained using $P(\mathbf{r})C(\mathbf{r}, t_D)$ (in general $P_{\text{open}}(\mathbf{r}, t_D) < P(\mathbf{r})C(\mathbf{r}, t_D)$).

In previous studies, we have only obtained the results in the top two rows of Table 3. The last two rows represent the most accurate scenario assuming that the hydrodynamic flow is confined on the length scales in our system (the original study by Gov et al.[26] showed better fits to fluctuation data for length scales in the range of hundreds of nanometers to microns, a range larger than for our relevant length scale of $\sim L_c$). In the case where $P(\mathbf{r})C(\mathbf{r}, t_D)$ is used, the increase in decay times due to the wall is roughly canceled by a decrease due to the smaller viscosity of water. The final values for the last two rows is approximately the same as for the first two rows. For the case where we use $P_{\text{open}}(\mathbf{r}, t_D)$, the values in the last two rows are about 3 or 4 times smaller than the first two rows. This decrease results from the fact that using $\eta^+ \neq \eta^-$ has a more drastic effect than in the previous case and is not canceled by the presence of the wall. Short time fluctuations are important in the case where we require the membrane to be above $h_0$ for the entire interval, and therefore it is not surprising that decreasing the viscosity above the bilayer leads to a larger reduction in the value of the macroscopic diffusion constant. In the scenario of the last two rows, as for the results of the previous study, the experimental value, $D_{\text{macro}} = 6.6 \times 10^{-3}\ \mu\text{m}^2\ \text{s}^{-1}$, lies between the values obtained using the two different methods. In this sense, the contributions of the wall and unequal viscosities largely cancel one another.

## IX. Conclusion

The computational limitations of molecularly based simulation schemes dictate that simpler models be developed to study phenomena over the length and time scales relevant to cellular biology and related physical systems. In this work we have extended the generality of the FSBD approach for modeling elastic membrane sheets by incorporating the possibility of noninfinite hydrodynamic environments. Although the resulting equations and algorithms are largely unaltered from the original FSBD methodology, the observation that generalized hydrodynamic kernels may be incorporated within this approach greatly enhances the practical utility of FSBD. We have presented two applications that clearly demonstrate the considerable influence of hydrodynamic conditions on membrane dynamics. Given the finite size and complex structures inherent to cellular systems, it is clear that noninfinite boundary conditions are a necessity to properly model most dynamics relevant to biology at the cellular scale.

**Acknowledgment.** This work was supported by the NSF (CHE-0349196, CHE-0321368). F.B. is an Alfred P. Sloan research fellow. We thank Jay Groves and Yoshihisa Kaizuka for providing us with their data. We also thank Rony Granek for helpful discussions.

## Appendix

We describe in more detail the diagonalization procedure used in the Harmonic Interactions section. The first step is to write eq 35 in terms of the $N^2$ independent modes $(\{a_{\mathbf{q}_c}\},\{a_{\mathbf{q}_r}\},\{b_{\mathbf{q}_c}\})$ defined in the section Independent Modes. All quantities in the new equations are explicitly real. It is

then necessary to rescale the modes such that both the Hamiltonian and the equation of motion can be simultaneously diagonalized. The appropriate set of variables is

$$\mathbf{c}^{\mathrm{T}} \equiv \left( \left\{ \frac{a_{\mathbf{q}_c}}{\sqrt{\Lambda_{\mathbf{q}_c}}} \right\}, \left\{ \frac{a_{\mathbf{q}_r}}{\sqrt{2\Lambda_{\mathbf{q}_r}}} \right\}, \left\{ \frac{b_{\mathbf{q}_c}}{\sqrt{\Lambda_{\mathbf{q}_c}}} \right\} \right) \tag{50}$$

with a new random force is similarly defined as

$$\mathbf{p}^{\mathrm{T}} \equiv \left( \left\{ \frac{f_{\mathbf{q}_c}}{\sqrt{\Lambda_{\mathbf{q}_c}}} \right\}, \left\{ \frac{f_{\mathbf{q}_r}}{\sqrt{2\Lambda_{\mathbf{q}_r}}} \right\}, \left\{ \frac{g_{\mathbf{q}_c}}{\sqrt{\Lambda_{\mathbf{q}_c}}} \right\} \right) \tag{51}$$

where each component obeys

$$\langle p_{\mathbf{q}}(t) \rangle = 0$$

$$\langle p_{\mathbf{q}}(t) p_{\mathbf{q}}(t') \rangle = k_B T L^2 \, \delta(t - t') \tag{52}$$

In terms of these new variables, the equations become

$$H = \frac{1}{L^2} (\mathbf{c}^{\mathrm{T}} \mathbf{M} \mathbf{c} + 2\mathbf{m}^{\mathrm{T}} \mathbf{c})$$

$$\frac{\partial \mathbf{c}(t)}{\partial t} = -\mathbf{M}\mathbf{c}(t) - \mathbf{m} + \mathbf{p}(t) \tag{53}$$

where matrix multiplication is implied. The vector $\mathbf{m}$ is defined by

$$\mathbf{m}^{\mathrm{T}} = \frac{\gamma L^2}{2} \sum_i (h_{\mathrm{cm}} - z_i) \, \mathbf{w}(\mathbf{R}_i) \tag{54}$$

where

$$\mathbf{w}(\mathbf{r}) = \frac{2}{L^2} \left( \{ \sqrt{\Lambda_{\mathbf{q}_c}} \cos(\mathbf{q}_c \cdot \mathbf{r}) \}, \left\{ \sqrt{\frac{\Lambda_{\mathbf{q}_r}}{2}} \cos(\mathbf{q}_r \cdot \mathbf{r}) \right\}, \{ -\sqrt{\Lambda_{\mathbf{q}_c}} \sin(\mathbf{q}_c \cdot \mathbf{r}) \} \right) \tag{55}$$

The matrix $\mathbf{M}$ is defined to be

$$\mathbf{M} = \begin{pmatrix} \mathbf{P} + \mathbf{Q} & \sqrt{2}\mathbf{Q} & -\mathbf{R} + \mathbf{S} \\ \sqrt{2}\mathbf{Q} & \mathbf{P} & \sqrt{2}\mathbf{S} \\ \mathbf{R} + \mathbf{S} & \sqrt{2}\mathbf{S} & \mathbf{P} - \mathbf{Q} \end{pmatrix} \tag{56}$$

$$P_{\mathbf{q}\mathbf{q}'} = \sqrt{\Lambda_{\mathbf{q}} \Lambda_{\mathbf{q}'}} \left[ (\kappa q^4 + \sigma q^2) \delta_{\mathbf{q},\mathbf{q}'} + \frac{\gamma}{L^2} \sum_i \cos[(\mathbf{q} - \mathbf{q}') \cdot \mathbf{R}_i] \right]$$

$$Q_{\mathbf{q}\mathbf{q}'} = \sqrt{\Lambda_{\mathbf{q}} \Lambda_{\mathbf{q}'}} \left( \frac{\gamma}{L^2} \sum_i \cos[(\mathbf{q} + \mathbf{q}') \cdot \mathbf{R}_i] \right)$$

$$R_{\mathbf{q}\mathbf{q}'} = \sqrt{\Lambda_{\mathbf{q}} \Lambda_{\mathbf{q}'}} \left( -\frac{\gamma}{L^2} \sum_i \sin[(\mathbf{q} - \mathbf{q}') \cdot \mathbf{R}_i] \right)$$

$$S_{\mathbf{q}\mathbf{q}'} = \sqrt{\Lambda_{\mathbf{q}} \Lambda_{\mathbf{q}'}} \left( -\frac{\gamma}{L^2} \sum_i \sin[(\mathbf{q} + \mathbf{q}') \cdot \mathbf{R}_i] \right) \tag{57}$$

where indices along each dimension are as defined in eq 31. For example, the block defined by $\mathbf{P} + \mathbf{Q}$ has dimensions of $(N^2 - 4)/2$ by $(N^2 - 4)/2$ and indices running through $\{\mathbf{q}_c^{\mathrm{real}}\}$ and $\{\mathbf{q}_c^{\mathrm{real}}\}$, the block defined by $-\mathbf{R} + \mathbf{S}$ has dimensions of $(N^2 - 4)/2$ by $(N^2 - 4)/2$ and indices running through $\{\mathbf{q}_c^{\mathrm{real}}\}$ and $\{\mathbf{q}_c^{\mathrm{imag}}\}$, the block defined by $\mathbf{P}$ has dimensions of $3 \times 3$ and indices running through $\{\mathbf{q}_r\}$ and $\{\mathbf{q}_r\}$, and the block defined by $\sqrt{2}\mathbf{P}$ has dimensions of $(N^2 - 4)/2 \times 3$ and indices running through $\{\mathbf{q}_c^{\mathrm{real}}\}$ and $\{\mathbf{q}_r\}$ (for the block in the first row, second column in $\mathbf{M}$). Note that the matrix $\mathbf{M}$ is a symmetric matrix resulting from the fact that $\mathbf{P}$, $\mathbf{Q}$, and $\mathbf{S}$ are symmetric and $\mathbf{R}$ is antisymmetric.

Diagonalization of $\mathbf{M}$ yields a transformation matrix $\mathbf{U}$, a set of eigenmodes $\mathbf{d} \equiv \mathbf{U}^{1-}\mathbf{c}$, and a set of eigenvalues $\omega$. Rewriting the equations in terms of these quantities and defining $\mathbf{n} \equiv \mathbf{U}^{-1}\mathbf{m}$ and $\mathbf{s} \equiv \mathbf{U}^{-1}\mathbf{p}$, we derive eq 38. Finally, to compute averages, an expression for $h(\mathbf{r})$ in terms of the eigenmodes is required. By defining $\mathbf{v}(\mathbf{r}) = \mathbf{w}(\mathbf{r})\mathbf{U}$, we can write the height as $h(\mathbf{r}) = \mathbf{v}(\mathbf{r})\mathbf{d}$. This definition of $\mathbf{v}(\mathbf{r})$ is used in eq 44.

## References


(1) Brannigan, G.; Lin, L. C.-L.; Brown, F. L. H. *Eur. Biophys. J.* **2006**, *35*, 104.

(2) Shelley, J. C.; Shelley, M. Y.; Reeder, R. C.; Bandyopadhyay, S.; Klein, M. L. *J. Phys. Chem B* **2001**, *105*, 4464.

(3) Marrink, S.; de Vries, A.; Mark, A. E. *J. Phys. Chem. B* **2004**, *108*, 750.

(4) Izvekov, S.; Voth, G. A. *J. Phys. Chem. B* **2005**, *109*, 2469.

(5) Smit, B.; Hilbers, P.; Esselink, K.; Rupert, L.; van Os, N.; Schlijper, A. G. *J. Phys. Chem* **1991**, *95*, 6361.

(6) Goetz, R.; Lipowsky, R. *J. Chem. Phys.* **1998**, *108*, 7397.

(7) Groot, R. D.; Rabone, K. L. *Biophys. J.* **2001**, *81*, 725.

(8) Ayton, G.; Bardenhagen, S. G.; McMurty, P.; Sulsky, D.; Voth, G. A. *J. Chem. Phys.* **2001**, *114*, 6913.

(9) Soddemann, T.; Dunweg, B.; Kremer, K. *Eur. Phys. J. E* **2001**, *6*, 409.

(10) Shillcock, J.; Lipowsky, R. *J. Chem. Phys.* **2002**, *117*, 5048.

(11) Yamamoto, S.; Maruyama, Y.; Hyodo, S.-A. *J. Chem. Phys.* **2002**, *116*, 5842.

(12) Rekvig, L.; Kranenburg, M.; Vreede, J.; Hafskjold, B.; Smit, B. *Langmuir* **2003**, *19*, 4897.

(13) Laradji, M.; Kumar, P. S. *Phys. Rev. Lett.* **2004**, *93*, 198105.

(14) Stevens, M. J. *J. Chem. Phys.* **2004**, ***121***, 11942.

(15) Farago, O. *J. Chem. Phys.* **2003**, *119*, 596.

(16) Brannigan, G.; Brown, F. L. H. *J. Chem. Phys.* **2004**, *120*, 1059.

(17) Brannigan, G.; Philips, P. F.; Brown, F. L. *Phys. Rev. E* **2005**, *72*, 011915.

(18) Cooke, I. R.; Kremer, K.; Deserno, M. *Phys. Rev. E* **2005**, *72*, 011506.

(19) Wang, Z.; Frenkel, D. *J. Chem. Phys.* **2005**, *135*, 234711.

(20) Canham, P. B. *J. Theor. Biol.* **1970**, *26*, 61.

(21) Helfrich, W. *Z. Naturforsch.* **1973**, *28c*, 693.

(22) Safran, S. A. *Statistical Thermodynamics of Surfaces, Interfaces and Membranes*; Westview Press: Boulder, CO, 1994.

(23) Brochard, F.; Lennon, J. F. *J. Phys. (Paris)* **1975**, *36*, 1035.

(24) Granek, R. *J. Phys. II (Paris)* **1997**, *7*, 1761.

(25) Zilman, A. G.; Granek, R. *Phys. Rev. Lett.* **1996**, *77*, 4788.

(26) Gov, N.; Zilman, A. G.; Safran, S. *Phys. Rev. Lett.* **2003**, *90*, 228101.

(27) Granek, R.; Klafter, J. *Europhys. Lett.* **2001**, *56*, 15.

(28) Gouliaev, N.; Nagle, J. F. *Phys. Rev. E* **1998**, *58*, 881.

(29) Gouliaev, N.; Nagle, J. F. *Phys. Rev. Lett.* **1998**, *81*, 2610.

(30) Lipowsky, R.; Zielenska, B. *Phys. Rev. Lett.* **1989**, *62*, 1572.

(31) Weikl, T. R.; Lipowsky, R. *Langmuir* **2000**, *16*, 9338.

(32) Lin, L. C.-L.; Brown, F. L. H. *Biophys. J.* **2004**, *86*, 764.

(33) Lin, L. C.-L.; Brown, F. L. H. *Phys. Rev. Lett.* **2004**, *93*, 256001.

(34) Lin, L. C.-L.; Brown, F. L. H. *Phys. Rev. E* **2005**, *72*, 011910.

(35) Seifert, U. *Phys. Rev. E* **1994**, *49*, 3124.

(36) Gov, N.; Zilman, A. G.; Safran, S. A. *Phys. Rev. E* **2004**, *70*, 011104.

(37) Kaizuka, Y.; Groves, J. T. *Biophys. J.* **2004**, *86*, 905.

(38) Kaizuka, Y.; Groves, J. T. *Phys. Rev. Lett.*, in press.

(39) Purcell, E. M. *Am. J. Phys.* **1977**, *45*, 3.

(40) Doi, M.; Edwards, S. F. *The Theory of Polymer Dynamics*; Clarendon Press: Oxford, 1986.

(41) van Kampen, N. G. *Stochastic Processes in Physics and Chemistry*; North-Holland: Amsterdam, 1992; pp 63, 83, 220−221.

(42) Happel, J.; Brenner, H. *Low Reynolds number hydrodynamics*; Kluwer: The Hague, The Netherlands, 1983.

(43) Ermak, D. L.; McCammon, J. A. *J. Chem. Phys.* **1978**, *69*, 1352.

(44) Sackmann, E. *Science* **1996**, *271*, 43.

(45) Sackmann, E.; Tanaka, M. *Trends Biotechnol.* **2000**, *18*, 58.

(46) Grakoui, A.; Bromley, S. K.; Sumen, C.; Davis, M. M.; Shaw, A. S.; Allen, P. M.; Dustin, M. L. *Science* **1999**, *285*, 221.

(47) Brian, A.; McConnell, H. M. *Proc. Natl. Acad. Sci.* **1984**, *81*, 6159.

(48) Lambacher, A.; Fromhertz, P. *Appl. Phys. A* **1996**, *63*, 207.

(49) Parthasarathy, R.; Groves, J. T. *Cell Biochem. Biophys.* **2004**, *41*, 391.

(50) Lin, L. C.-L.; Brown, F. L. H. Submitted for publication.

(51) Brown, F. L. H. *Biophys. J.* **2003**, *84*, 842.

(52) Cherry, R. J. *Biochim. Biophys. Acta* **1979**, *559*, 289.

(53) Schindler, M.; Koppel, D. E.; Sheetz, M. P. *Proc. Natl. Acad. Sci. U.S.A.* **1980**, *77*, 1457.

(54) Sheetz, M. P.; Schindler, M.; Koppel, D. E. *Nature* **1980**, *285*, 510.

(55) Koppel, D. E.; Sheetz, M. P.; Schindler, M. *Proc. Natl. Acad. Sci. U.S.A.* **1981**, *78*, 3576.

(56) Sheetz, M. P. *Semin. Hematol.* **1983**, *20*, 175.

(57) Byers, T. J.; Branton, D. *Proc. Natl. Acad. Sci. U.S.A.* **1985**, *82*, 6153.

(58) Liu, S.; Derick, L.; Palek, J. *J. Cell. Biol.* **1987**, *104*, 527.

(59) Tomishige, M.; Sako, Y.; Kusumi, A. *J. Cell Biol.* **1998**, *142*, 989.

(60) Saffman, P. G.; Delbruck, M. *Proc. Natl. Acad. Sci. U.S.A.* **1975**, *73*, 3111.

(61) Tsuji, A.; Ohnishi, S. *Biochemistry* **1986**, *25*, 6133.

(62) Tsuji, A.; Kawasaki, K.; Ohnishi, S.; Merkle, H.; Kusumi, A. *Biochemistry* **1988**, *27*, 7447.

(63) Edidin, M.; Kuo, S. C.; Sheetz, M. P. *Science* **1991**, *254*, 1379.

(64) Corbett, J. D.; Agre, P.; Palek, J.; Golan, D. E. *J. Clin. Invest.* **1994**, *94*, 683.

(65) Kusumi, A.; Sako, Y. *Curr. Opin. Cell Biol.* **1996**, *8*, 566.

(66) Tomishige, M. Ph.D. Thesis, The University of Tokyo, 1997.

(67) Podgornik, R.; Parsegian, V. A. *Langmuir* **1992**, *8*, 557.

(68) Fournier, J.-B.; Lacoste, D.; Raphael, E. *Phys. Rev. Lett.* **2004**, *92*, 018102.

(69) Zhang, D.; Klyatkin, A.; Bolin, J. T.; Low, P. S. *Blood* **2000**, *96*, 2925.

CT050293S